

Thermal transport in SiGe superlattice thin films and nanowires: Effects of specimen and periodic lengths

Keng-Hua Lin and Alejandro Strachan

School of Materials Engineering and Birck Nanotechnology Center, Purdue University, West Lafayette, Indiana 47907, USA

(Received 3 April 2012; revised manuscript received 2 December 2012; published 4 March 2013)

We compute the thermal conductivity of superlattice (SL) thin films and nanowires for various SL periods and total specimen lengths using nonequilibrium molecular dynamics. Both types of materials exhibit similar behaviors with respect to SL period but the thermal conductivity of the thin films exhibits a significantly higher sensitivity to the specimen length. Notably, the thermal conductivity of SL thin films is smaller than those of the corresponding nanowires for specimen lengths below approximately 35 nm. These results arise from the complex dependence of the conductivities of the interfaces and the SL components on the specimen size and period. These trends and observations are explained using a simple phonon model that builds on the relationship between the cumulative thermal conductivity and the phonon wavelength.

DOI: [10.1103/PhysRevB.87.115302](https://doi.org/10.1103/PhysRevB.87.115302)

PACS number(s): 65.80.-g, 68.65.Cd, 63.22.-m, 63.22.Np

I. INTRODUCTION

Understanding the role of nanostructure on thermal transport and nanoengineering the desired behavior remain key challenges in condensed matter and materials physics with wide and important practical applications.¹⁻³ In the case of thermoelectric devices, a widely used dimensionless figure of merit, ZT , is defined as the ratio with the Seebeck coefficient (S), electrical conductivity (σ), and temperature (T) in the numerator and the thermal conductivity (κ) in the denominator: $\frac{S^2\sigma}{\kappa}T$. A successful approach to improve the performance of thermoelectric materials is to decrease the phonon thermal conductivity without negatively impacting the electrical conductivity or the Seebeck coefficient.⁴⁻⁶ This is possible via nanostructure development in materials with the mean-free paths of phonons longer than those of electrons and, therefore, defects can be engineered to scatter phonons predominantly.^{2,7-17} For example, electroless etched Si nanowires with rough surfaces exhibit a thermal conductivity as low as ~ 1 W/(m K):² a significant reduction compared to the thermal conductivity of bulk Si [142 W/(m K)¹⁸ at room temperature]. In addition, a room temperature phonon thermal conductivity of approximately 1.8 W/(m K) has been reported for an n -type SiGe alloy with fine grains.¹⁵ Core-shell nanowires (NWs)^{9,10} and superlattice (SL) materials^{7,8,11-14} have also attracted significant interest since interfaces promote the phonon scattering.

Superlattice or nanolaminate materials are attractive since their periodic lengths can be adjusted to maximize the phonon scattering, and several studies have focused on the role of SL periods on thermal transport, both experimentally^{7,8,11-14} and theoretically.¹⁹⁻²² For SiGe SL thin films (TFs), thermal conductivity on the order of 5 W/(m K) has been reported for various SL periods.^{7,12} Moreover, Si/SiGe SL nanowires show a lower thermal conductivity than Si/SiGe SL TFs and pure Si NWs with similar diameters.¹³ Regarding the effect of periodic lengths, both experimental and theoretical studies^{19-21,23,24} have shown that the thermal conductivity exhibits a minimum for a finite period. This optimal period has been associated with the transition between wave-like and particle-like transport behaviors of phonons.^{20,21}

Despite such progress, important aspects of the thermal transport in SL materials remain unclear. Key among these is the role of the specimen lengths in thermal transport of SL TFs and NWs. Many applications call for miniaturization and the specimen size becomes an important variable. Experimental^{25,26} and theoretical²⁷ studies have shown that thermal conductivity depends on the specimen size when it becomes comparable to the phonon mean-free path. Furthermore, recent simulation studies^{28,29} have reported that the total length of the specimens affects the interface resistivity and the thermal conductivity of individual layers in SLs.

In this paper we characterize how specimen and SL periodic lengths affect the response of SL TFs and SL NWs, and find that these two systems exhibit distinct behaviors. Interestingly, even though the thermal conductivity of SL TFs is higher than those of SL NWs for large specimen lengths, this relationship reverses at small scales. This surprising result indicates that the short SL TFs may be attractive candidates for thermoelectric applications as compared to the SL NWs. Section II of the paper describes simulation details and Sec. III presents results of thermal conductivity of pure Si and Ge bulk and nanowires to validate our approach and establish size effects in homogeneous systems. Section IV focuses on the central results of the paper, i.e., the size effects on SL structures, and Sec. V discusses the results. Finally, Sec. VI draws conclusions.

II. MODEL STRUCTURES AND SIMULATION METHODOLOGY

All molecular dynamics (MD) simulations are performed using LAMMPS, a parallel simulator from Sandia National Laboratory.³⁰ We use the Stillinger-Weber potential to describe the interaction between Si and Ge atoms. The potential includes 2-body and 3-body terms for Si and Ge as described in Refs. 31,32, and the combination rules are used to determine the Si-Ge cross interactions. As described in Ref. 19, the arithmetic average is used for the distance parameter ($\sigma_{\text{Si-Ge}}$) and the geometric average is used for the energy parameters ($\epsilon_{\text{Si-Ge}}$ and $\lambda_{\text{Si-Ge}}$).

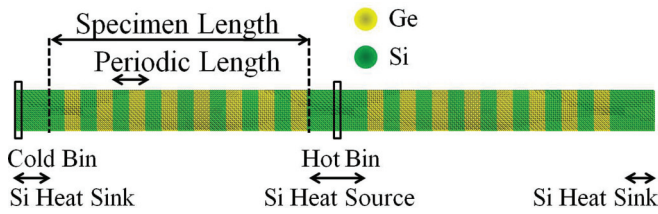


FIG. 1. (Color online) Longitudinal view of superlattice thin films and nanowires. The structures consist of two segments of specimens, a heat source, and a heat sink. The heat is conducted along the z [001] direction.

A. Material structures and structural relaxation

We characterize the thermal conductivity of pure Si and Ge bulk systems, square NWs, and circular NWs, as well as SiGe SL TFs and NWs. In all cases, thermal transport is studied along the [001] crystallographic direction. For pure Si and Ge bulks, the lattice parameters are 0.543 nm and 0.565 nm, respectively. The SL TFs consist of alternating Si and Ge layers with periodic lengths ranging from 0.275 nm (0.5 unit cells) to 35.235 nm (64 unit cells). The initial in-plane lattice parameter for the SL TFs (along x and y) is set to 0.554 nm, the average between the Si and Ge lattice parameters. From elasticity theory, the relaxed lattice parameters along the heat transport direction (z) are 0.535 nm and 0.574 nm for Si and Ge, respectively, and this is used to generate the initial configuration of the SL TFs. For SL TFs with periodic lengths smaller than one unit cell, the average a_z of 0.554 nm is used for both Si and Ge layers. Since thermal conductivity is size dependent when the material sizes are comparable to the phonon mean-free path, we study specimens with various lengths along the z direction, as listed in Table I. These structures include two Si heat baths ($10 \times 10 \times 15$ unit cells each) and two segments of materials (bulk/SLs) as shown in Fig. 1.

All structures are relaxed and thermalized before thermal conductivity simulations. This is particularly important in the SL calculations where long-lived, noncanonical waves can develop due to acoustic and lattice mismatch between Si and Ge. We use the following procedure: (i) isothermal-isobaric (NPT) simulation with temperature ramping from 10 K to 300 K in 100 ps; (ii) NPT simulation at 300 K for 50 ps; (iii) isothermal-isochoric (NVT) simulations at 300 K for 100 ps with simulation cell parameters obtained over the last 10 ps of step (ii). Velocities are reassigned every 10 ps to disperse the coherent waves in the SL TFs in step (iii). These relaxation steps are essential particularly for SL TFs with large periodic lengths. A time step of 0.5 fs and 3D periodic boundary conditions are applied to these relaxation procedures.

In order to create NW structures, the fully thermalized Si and Ge bulk systems and SiGe SL TFs are replicated twice along the x and y directions, and NWs with square and circular cross sections are carved out from these simulation cells. The NWs contain the same number of atoms as their bulk or TF counterparts. Free boundary conditions are applied to the x and y directions, and periodic boundary conditions are maintained along the z direction. Relaxation steps (ii) and (iii) mentioned before are applied to these structures. The dimensions and the total numbers of atoms for pure Si and Ge structures are summarized in Table I, and those for SiGe SL TFs and NWs are summarized in Table II. We note that our SL systems have defect-free, coherent interfaces. This is justified since the critical thickness for coherency loss in SiGe SL TFs is tens of nanometers,³³ and the strain relaxation through the free surfaces of NWs further increase this critical thickness.³⁴

B. Thermal conductivity calculation

We use a nonequilibrium method proposed by Müller-Plathe³⁵ to compute the thermal conductivity in various specimens of interest. In this approach, a heat flux (J) is introduced into the system, and a 1D temperature gradient ∇T developed is determined from the atomic velocities. The thermal conductivity (κ) is then computed by Fourier's law:

$$\kappa = -\frac{J}{\nabla T}. \quad (1)$$

To introduce a heat flux, the system is divided into N bins along the transport direction. Bin 1 is designated as the cold bin and bin $N/2 + 1$ is designated as the hot bin. These bins are in the center of Si heat source/sink. The heat flux is generated by periodically exchanging the velocities of the hottest atom in the cold bin with the coldest atom in the hot bin. In these simulations we use a time step of 2 fs and in all cases velocity exchanges are conducted every 200 fs (100 MD steps); under these conditions, the heat flux generated is in the range $(2.0\text{--}2.7) \times 10^9$ W/m², comparable to the previous studies.^{36,37} The temperature gradients achieve steady state after 1 ns and the temperature differences between the hot and cold bins are in the range of 60–120 K. Under these conditions the system remains in the linear regime between heat flux and temperature gradient as detailed in the Supplemental Material.³⁸ The thermal conductivity is calculated by averaging the heat flux and ∇T from 1 ns to 4.8 ns. An overall thermostat (NVT ensemble) is applied to the system to maintain the overall temperature at $T = 300$ K and to avoid drifts in such long simulations. The thermostat damping time is set to 20 ps, and this represents weak coupling to avoid interfering with the thermal transport.

TABLE I. Dimensions and numbers of atoms for pure Si and Ge bulks, square nanowires, and circular nanowires.

	Cross-Sectional Area (nm ²)	Specimen Length (nm)	Number of Atoms
Bulk	Si: 29.5	Si: 27.2–146.8	40000–216000
	Ge: 32.0	Ge: 28.3–152.9	
Square/circular NWs	Si: 31.7–72.1	Si: 27.0–146.4	40000–486000
	Ge: 34.2–79.4	Ge: 28.2–152.2	

TABLE II. Dimensions and numbers of atoms for SiGe superlattice thin films, square nanowires, and circular nanowires.

Cross-Sectional Area (nm ²)	Specimen Length (nm)	Periodic Length (nm)	Number of Atoms
Thin films: 33.4	86.7–228.0	0.3–35.2	126400–331200
Nanowires: 33.5–36.6			

These predictions are based on classical molecular dynamics and therefore neglect quantum effects. This is justified since quantum effects affect predominantly high-frequency modes that play a small role in thermal transport; thus quantum effects on thermal conductivity of Si at 300 K are small.^{19,39,40}

III. SIZE EFFECT IN PURE Si AND Ge BULK AND NANOWIRES

Figure 2 characterizes specimen size effect on the thermal conductivity in pure Si and Ge samples. We show the inverse thermal conductivity of Si [Fig. 2(a)] and Ge [Fig. 2(b)] bulk systems and NWs as a function of inverse specimen lengths (taken as $1/L_z$). The hot and cold bins in the simulations provide constraints to the phonon mean-free path and their separation provides a measure of specimen size.

Based on the kinetic theory, the size effect on thermal conductivity can be approximated by the following relationship:^{27,37}

$$\frac{1}{\kappa} = \frac{3}{Cv} \left(\frac{1}{l_\infty} + \frac{1}{l_z} \right), \quad (2)$$

where C is the specific heat, v is the phonon group velocity of the material, and l_∞ is the phonon mean-free path for infinite specimen length. More accurate descriptions involve sums over wave vector or frequency of a mode specific heat capacity and mean-free path;⁴¹ however, we find this

approximate relationship appropriate for the purpose at hand. The intrinsic thermal conductivity and the average mean-free paths shown in Table III are obtained by fitting the MD data of the longest three samples presented in Fig. 2 using Eq. (2). Before moving on to SL results we discuss the accuracy of the predictions and the trends observed in these homogeneous materials. The calculated thermal conductivity and the average phonon mean-free path for pure bulk Si are 140 ± 4 W/(m K) and 130 ± 10 nm, respectively. The thermal conductivity is very close to the experimental value of 142 W/(m K).¹⁸ Since the definition of phonon mean-free path varies in different studies, we compare our values to some reported numbers here. The phonon mean-free path we obtained is close to the value of 115 nm, obtained from the ratio of the experimental thermal conductivity to the calculated thermal conductance per unit area using the Landauer formalism.⁴² Experimentally, an effective phonon mean-free path of 300 nm for Si has been reported²⁵ as the thickness of the Si thin film with one half of its bulk thermal conductivity. From our results, the thickness of the Si film to achieve the half bulk thermal conductivity is 134 nm, approximately half of the value reported in Ref. 25. For pure bulk Ge, the calculated thermal conductivity and the average phonon mean-free path are 93 ± 1 W/(m K) and 117 ± 4 nm. The calculated thermal conductivity for Ge is slightly higher than the experimental result, 58 W/(m K).⁴³ The experimental thermal conductivity of Si⁴⁴ and Ge⁴⁵ films with thicknesses of 500 and 900 nm are also shown in Figs. 2(a) and 2(b) as green squares.

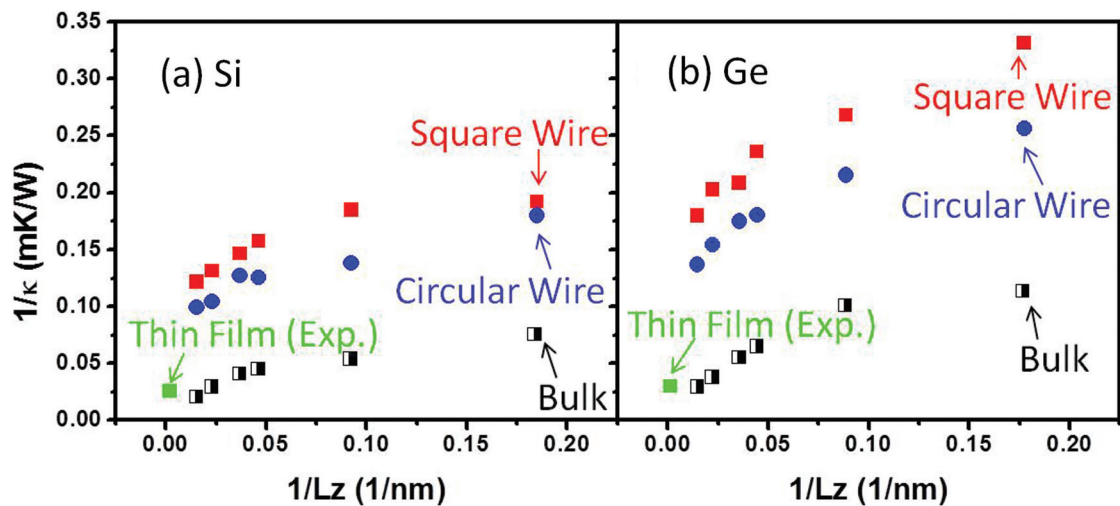


FIG. 2. (Color online) Relation between the inverse specimen lengths and the inverse thermal conductivity for (a) pure Si and (b) pure Ge structures. The thermal conductivity of the bulks with cross sections of 29.5 nm² is plotted in black half right squares. The thermal conductivity of square and circular nanowires with the same number of atoms as the bulks is plotted in red squares and blue circles, respectively. “Bulk” refers to the systems with 3D periodic boundary condition, and L_z is the real specimen length of these systems along the heat transport direction. The experimental thermal conductivity of Si and Ge films with thicknesses of 500 nm (Ref. 44) and 900 nm (Ref. 45), respectively, is plotted in green squares.

TABLE III. Phonon mean-free paths and intrinsic thermal conductivity of pure Si, Ge bulks, and square and circular nanowires. The experimental values are also shown in parentheses.

	Si		Ge	
	κ [W/(m K)]	Average Phonon Mean-Free Path (nm)	κ [W/(m K)]	Average Phonon Mean-Free Path (nm)
Bulk	140 ± 4 (Exp.: 142 ¹⁸)	130 ± 10 (Exp.: 300 ²⁵)	93 ± 1 (Exp.: 58 ⁴³)	117 ± 4
Square nanowire	9.6 ± 0.1	11 ± 0.3	6 ± 0.1	8 ± 4
Circular nanowire	13 ± 1.1	17 ± 3.2	9 ± 0.0	16 ± 2

Figures 2(a) and 2(b) also show that the thermal conductivity of Si NWs (with circular cross section of radius 3.18 nm and square cross section of width 5.87 nm) and Ge NWs (with circular cross section of radius 3.30 nm and square cross section of width 6.12 nm). The inverse conductivity of NWs is about a factor of two higher than their bulk counterparts. Inelastic surface scattering and the effect of free surfaces and finite size on phonon properties contribute to the low thermal conductivity of NWs. As expected, the reduction in thermal conductivity and phonon mean-free paths is more prominent for square NWs than for circular ones due to the larger surface-to-volume ratios and the sharp corners of square NWs; this is consistent with prior results.⁴⁶ The average phonon mean-free paths extracted from the data in Fig. 2 are from 8 nm for Ge square NW to 17 nm for Si circular NW, i.e., slightly larger than the widths or diameters of the NWs. Figure 3 shows the thermal conductivity (a) and average phonon mean-free paths (b) as a function of NW width/diameter. Our MD simulations predict a linear increase in conductivity and mean-free path with widths/diameters, in agreement with the trends of experimental results.²

From our simulations, the intrinsic thermal conductivity extrapolated from the data of finite-size specimens agrees with the experimental results well for both Si and Ge. However, in direct comparisons of Si and Ge NWs and films to the experimental results, our simulations overestimate the thermal conductivity. This may be due to the defect-free, highly purified, and single-crystalline characters of the MD structures.

IV. Si/Ge SUPERLATTICE THIN FILMS AND NANOWIRES

The average temperature profiles of SiGe SL TFs and NWs with periodic lengths of approximately 4.4 nm are shown in Fig. 4. We observe linear temperature profiles away from the two heat baths used to generate the heat flux; the slope of the temperature profile is steeper near the two specimen ends. The results shown below are obtained from the temperature gradients obtained excluding only the Si heat baths; this region is marked as “SL” in Fig. 4. The thermal conductivity of the specimens calculated from the linear temperature region (excluding the first interface³⁸ near the heat baths) is shown in the Supplemental Material³⁸ and exhibits the same trend.

Figure 5 shows the thermal conductivities of the SiGe SL TFs and NWs as a function of SL periods for three specimen lengths. The results in Fig. 5 can also be simulated by MD simulation tool “nanoMATERIALS nanoscale heat transport” with a user-friendly interface on nanoHUB.⁴⁷ Experimental results for SiGe SL TFs^{7,12} are also included in Fig. 5 for validation. We see that the predicted thermal conductivity is in good agreement with the experiments.^{7,12} As expected from the prior simulations and experiments,^{21,24} our results show a minimum thermal conductivity for the SLs with finite periods. The minimum occurs at periods of 8.82 nm, 2.20 nm, and 2.20 nm for SiGe SL TFs, square NWs, and circular NWs, respectively. Simkin *et al.*²¹ proposed that periodic lengths corresponding to minimum thermal conductivity mark the transition between particle-like and wave-like transport behavior of phonons. According to this explanation, in the particle-like transport regime the thermal conductivity

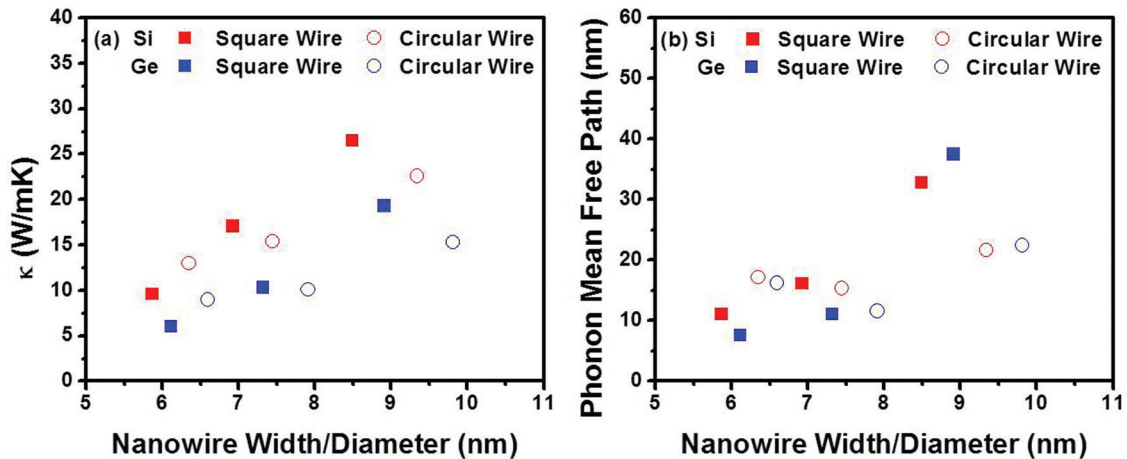


FIG. 3. (Color online) (a) Thermal conductivity and (b) phonon mean-free paths of pure Si and Ge square/circular nanowires with different widths/diameters.

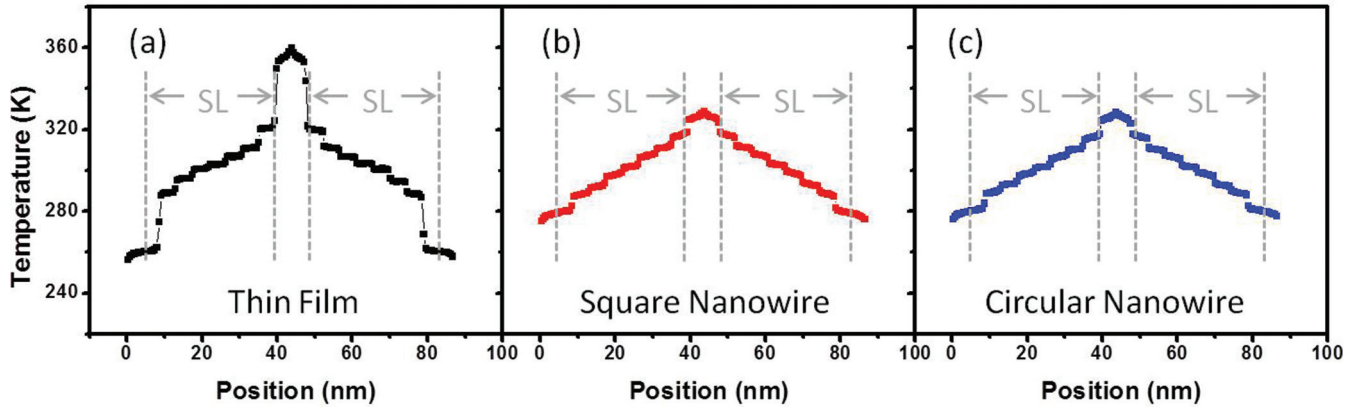


FIG. 4. (Color online) Temperature profiles of SiGe superlattice (a) thin films, (b) square nanowires, and (c) circular nanowires with periodic lengths of approximately 4.4 nm. The SL regimes are applied in calculating the temperature gradients.

decreases with decreasing periodic length due to the enhanced interface scattering. In the wave-like regime, transport is dominated by phonons that *see* the lattice as a uniform material and are not scattered by interfaces. Our results show that the minimum thermal conductivity of SL TFs occurs at a larger period than SL NWs; this phenomenon will be discussed in Sec. V.

The most significant result in Fig. 5 is, however, that the thermal conductivity of the SL TFs is much more sensitive to specimen lengths than those of the SL NWs. For relatively long specimens (approximately 100 nm), the thermal conductivity of the SL TFs is significantly larger than that of the NWs; this result is consistent with the observations in pure Si and Ge cases. However, for 35-nm-long specimens, the NWs conduct better than the SL TFs for some SL periods.

To better quantify the results, we compare the thermal conductivity of SL TFs and NWs of the same specimen length in Fig. 6. From Figs. 6(b) and 6(c), we see that for specimens longer than 70 nm, the SL TFs have higher thermal conductivity than the NWs for all periods. However, in Fig. 6(a), for the 35-nm-long specimens, the thermal conductivity of the SL TFs is smaller than that of the NWs for periodic lengths exceeding 10 nm. The relationship between thermal conductivity and specimen length for specimens with different periodic lengths is also included in the Supplemental Material.³⁸

To understand the origin of such interesting physics, the thermal conductivity of the overall specimen, κ , is described by the temperature drops contributed by the individual Si and Ge layers (ΔT_{Si} and ΔT_{Ge}), and by the interfaces ($\Delta T_{\text{interface}}$) between them as follows:

$$\begin{aligned} \frac{1}{\kappa} &= -\frac{\Delta T}{L_{\text{specimen}} J} = -\frac{\sum_{\text{layers}} \Delta T_{\text{Si}} + \sum_{\text{layers}} \Delta T_{\text{Ge}} + \sum_{\text{interfaces}} \Delta T_{\text{interface}}}{L_{\text{specimen}} J} \\ &= -\frac{\sum_{\text{layers}} \nabla T_{\text{Si}} L_{\text{Si}} + \sum_{\text{layers}} \nabla T_{\text{Ge}} L_{\text{Ge}} + \sum_{\text{interfaces}} \frac{\Delta T_{\text{interface}}}{a_z} a_z}{L_{\text{specimen}} J} \\ &= \sum_{\text{layers}} \frac{1}{\kappa_{\text{Si}}} \frac{L_{\text{Si}}}{L_{\text{specimen}}} + \sum_{\text{layers}} \frac{1}{\kappa_{\text{Ge}}} \frac{L_{\text{Ge}}}{L_{\text{specimen}}} + \sum_{\text{interfaces}} \rho_{\text{interface}} \frac{a_z}{L_{\text{specimen}}}, \end{aligned} \quad (3)$$

where ΔT is the temperature drop across the specimen length (L_{specimen}); L_{Si} and L_{Ge} are the lengths of Si and Ge layers. $\Delta T_{\text{interface}}$ is the temperature drop across the interfaces, and is the difference between the extrapolations of the linear fits of the temperature profiles from the two adjacent layers to the interfaces. Even though the interfaces have zero length, to make the expressions in Eq. (3) consistent, the lengths of the interfaces are assumed to be the same as the lattice parameter along the heat transport direction (a_z).

The thermal resistivity for Si and Ge layers, $\rho_{\text{Si(Ge)}}$, in Eq. (3) is defined as

$$\rho_{\text{Si(Ge)}} = \frac{1}{\kappa_{\text{Si(Ge)}}} = -\frac{\nabla T_{\text{Si(Ge)}}}{J}, \quad (4)$$

where $\kappa_{\text{Si(Ge)}}$ is the thermal conductivity of each Si or Ge layer. The interface resistivity, $\rho_{\text{interface}}$, in Eq. (3) between Si and Ge layers is defined as

$$\rho_{\text{interface}} = -\frac{\Delta T_{\text{interface}}/a_z}{J}. \quad (5)$$

Figure 7 shows the average thermal conductivity of the Si and Ge layers inside each SL TF and NW, and Fig. 8 shows the corresponding interface resistivity. Due to the different phonon properties in Si and Ge, the interface resistivity depends on the direction of the heat flow. Therefore, we separate these two cases in Fig. 8. We should note that both thermal conductivity and interface resistivity are temperature dependent,³⁷ but for a qualitative comparison, we use the average values here.

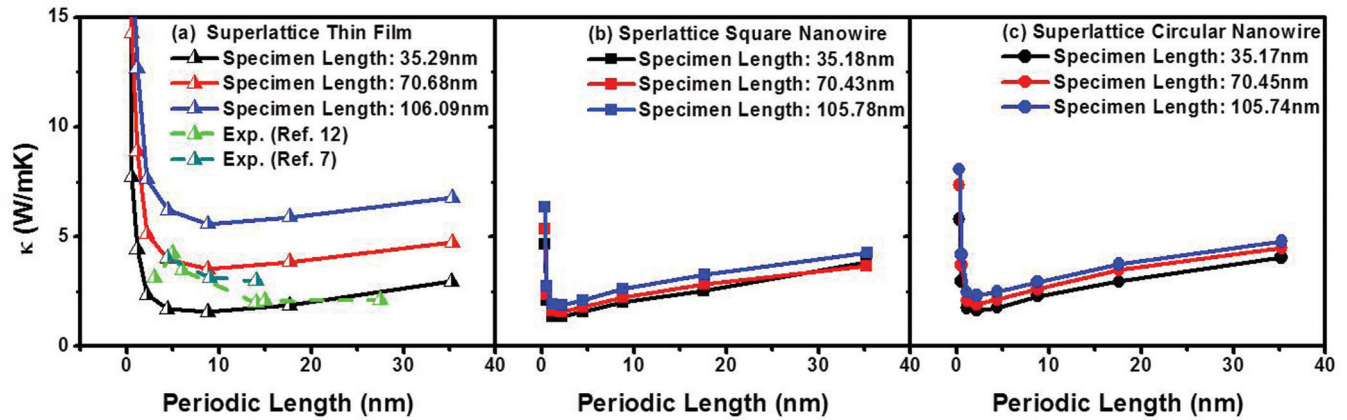


FIG. 5. (Color online) Thermal conductivity of SiGe superlattice (a) thin films, (b) square nanowires, and (c) circular nanowires with different specimen and periodic lengths. Experimental data of SiGe superlattice thin films (Refs. 7,12) are shown in (a) as a comparison.

From Figs. 7 and 8, the layer thermal conductivity and interface resistivity of SL TFs are more sensitive to the specimen and periodic lengths than the NW ones. The high interface resistivity in 35-nm-long TF specimens causes their thermal conductivity to be lower than that of NWs. As the specimen length increases, the interface resistivity of the TFs is significantly reduced, and therefore their overall thermal conductivity becomes larger than that of NWs. The origin of the high interface resistivity of TFs and the size dependence of the layer thermal conductivity and the interface resistivity will be discussed in the following section.

V. DISCUSSION: ROLE OF SPECIMEN AND PERIODIC LENGTH ON THERMAL CONDUCTION OF SUPERLATTICES

As shown in Sec. IV, the thermal conductivity of the SL TFs shows stronger dependence on specimen length than that of square and circular SL NWs. The results in Figs. 7 and 8 provide key insights into such size effects and the main observations from our MD results are as follows:

(i) The interface resistivity of both SL TFs and NWs increases with SL period; reducing specimen length leads to

a significant increase in interfacial resistivity in SL TFs and little change in NWs.

(ii) The conductivity of individual Si and Ge layers depends on the specimen lengths for the SL TFs (similar to the bulk cases); in the case of NWs they show little specimen size dependence.

(iii) The minimum thermal conductivity of SL TFs occurs at a larger periodic length than that of SL NWs.

We explain these observations via a simple phonon model using the cumulative thermal conductivity with respect to the phonon wavelength, λ . Phonons with different wavelengths contribute differently to the thermal conductivity of materials. Henry *et al.*^{5,41} calculate the cumulative phonon thermal conductivity with respect to the phonon wavelength of Si bulk at 300 K using lattice dynamics and MD. The resulting plots show that phonons with medium wavelengths dominate the thermal conductivity;⁴¹ this is because short-wavelength phonons are easily scattered and long-wavelength phonons are very few in number. The solid line in Fig. 9(a) shows schematically the cumulative phonon thermal conductivity of a SL TF as a function of the phonon wavelength based on the results by Henry *et al.*⁴¹ The corresponding curve for a NW (dashed line) can be expected to be similar to that of the TF for short-wavelength phonons (which are mostly unaware of

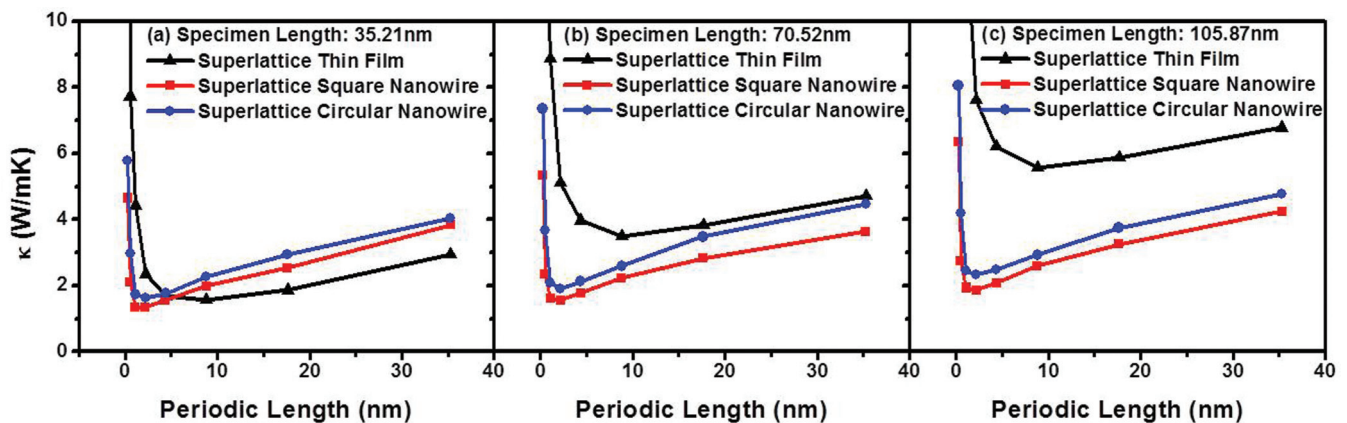


FIG. 6. (Color online) Thermal conductivity of superlattice thin films and square and circular nanowires with specimen lengths of (a) 35.21 nm, (b) 70.52 nm, and (c) 105.87 nm with various periodic lengths.

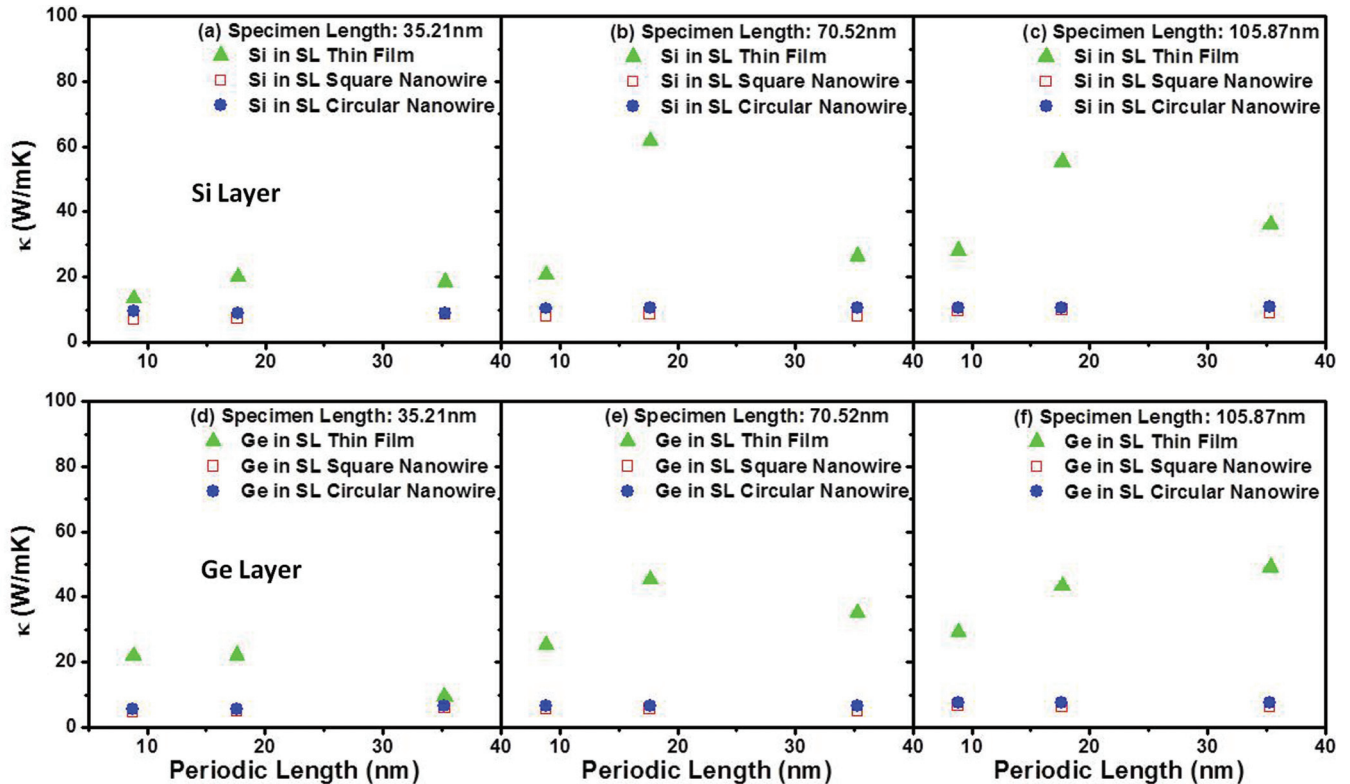


FIG. 7. (Color online) Thermal conductivity of Si/Ge layers inside superlattice thin films and square and circular nanowires with specimen lengths of (a), (d) 35.21 nm; (b), (e) 70.52 nm; and (c), (f) 105.87 nm.

the wire dimensions) but will increase to a smaller number, as the mean-free paths for the medium- and long-wavelength phonons are restricted [dashed line in Fig. 9(b)]. Figure 9(b) shows the same schematic curves but each is normalized by its corresponding total thermal conductivity. Two characteristic sizes should be considered to understand the size effects in SL structures. The specimen length imposes a maximum wavelength that can be supported by the material (L_{SP}); phonons with $\lambda > L_{SP}$ do not exist. The remaining phonons can be divided into two categories: (i) SL phonons with $L_{SP} > \lambda > L_{SL}$ (where L_{SL} is the SL periodic length); and (ii) sub-SL phonons with $L_{SL} > \lambda$. The sub-SL phonons, with wavelengths shorter than the periodic lengths, can be scattered by the interfaces and consequently are responsible for the interface resistivity. The SL phonons have wavelengths longer than the periodic lengths and, therefore, conduct heat without being scattered by the interfaces. While the categorization of phonons into these two groups is an oversimplification, the construct is useful to understand the relative importance of SL and sub-SL phonons as a function of the two characteristic length scales of the system.

Let us start with the first observation mentioned above, i.e., the sensitivity of interface resistivity to the specimen and periodic lengths and the high resistivity in SL TFs for short specimens. Atomic snapshots of the interfaces in SL TFs and NWs (included in the Supplemental Material³⁸) show coherent, atomically sharp interfaces in all cases. Thus, we do not expect the atomic detail of the interfaces to play a significant role and the size effects should be related to the nature of the phonons involved in heat transport. Figure 9 shows that decreasing the specimen length reduces the number

of SL phonons while the number of sub-SL phonons remains unchanged. Thus, the fraction of the energy transported by the sub-SL phonons increases and so does the interface resistivity as the specimen length decreases. The medium-to long-wavelength (10–100 nm) phonons in NWs contribute less to their thermal conductivity as compared to the TFs, explaining the lower sensitivity of NWs to the specimen length (Fig. 8). This explains why the interface resistivities of long-specimen SL TFs and NWs are similar, but TFs exhibit higher interface resistivity as the specimen length decreases. The effect of SL periodic length on interfacial resistivity can be explained in a similar manner. Decreasing the periodic length increases the number of SL phonons at the expense of sub-SL phonons. The decrease in the fraction of the total heat carried by the sub-SL phonons leads to the decrease in interface scattering as shown in Fig. 8.

The second observation mentioned above, i.e., the insensitivity of the thermal conductivity of the Si and Ge layers in the SL NWs, is due to the minimal contribution of phonons with wavelengths longer than L_{SL} to the NWs' thermal conductivity; see Fig. 9(b). In contrast, those phonons represent a larger fraction of the total heat transport in SL TFs and explain their significant specimen size effects. Another way to think about this phenomenon is that since SL NWs possess small average phonon mean-free paths as described in Sec. III, negligible size effects are expected due to the diffusive transport behavior.

The third observation is that the minimum thermal conductivity of SL TFs occurs for a larger periodic length than in SL NWs. This minimum is believed to occur when the SL

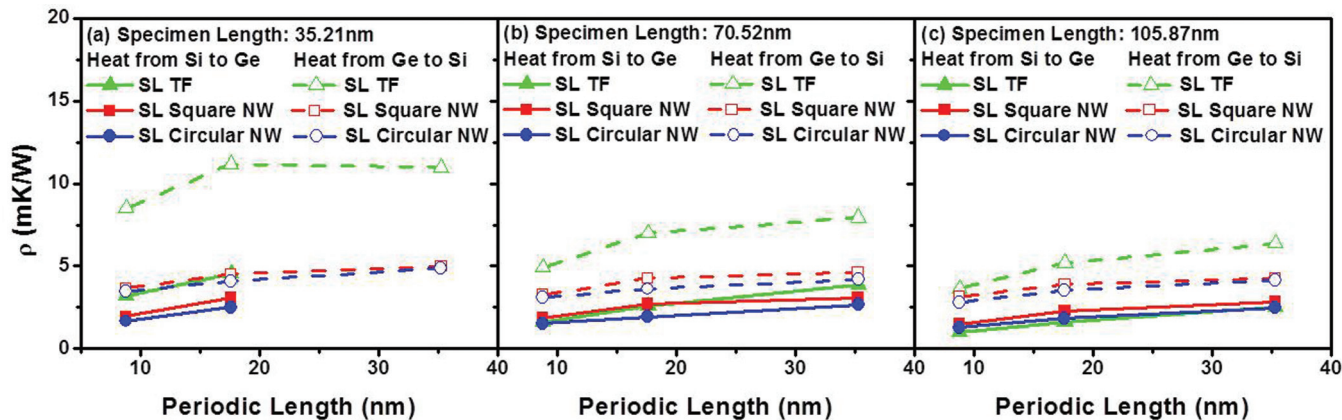


FIG. 8. (Color online) Interface resistivity between Si and Ge layers inside superlattice thin films and square and circular nanowires with specimen lengths of (a) 35.21 nm, (b) 70.52 nm, and (c) 105.87 nm. Heat transfers from Si to Ge are plotted with solid lines and solid symbols, and heat transfers from Ge to Si are plotted with dashed lines and open symbols.

phonons (which are not scattered by the interfaces) dominate the thermal transport; under these conditions further reduction in periodic length does not increase scattering significantly but increases the number of phonons that see the material as homogeneous. Figure 9(b) shows that this transition would occur for longer periodic length in the case of TFs as compared to NWs; this is because long-wavelength phonons contribute more to thermal transport in TFs. Experimental results on the specimen-size effects on thermal conductivity

in SL TFs were published during the final stages of review of this manuscript.⁴⁸ These results are consistent with the trends observed in our simulations.

VI. CONCLUSIONS

The thermal conductivity of various Si/Ge nanomaterials is calculated in this study from nonequilibrium MD simulations. Interface, specimen length, and SL periodic length all play important roles in thermal transport. For pure Si and Ge materials, the thermal conductivity and phonon mean-free paths increase with the specimen length, and the presence of the free surface in Si/Ge NWs significantly reduces the thermal conductivity as compared to their bulk counterparts. For SiGe SL TFs and NWs, both specimen and periodic lengths influence the thermal conductivity of materials. Since the enhanced surface scattering in SiGe SL NWs leads to a reduction in phonon mean-free path and more diffusive transport, the layer thermal conductivity and interface resistivity of SL NWs are less specimen-size-dependent than those of SL TFs. As the specimen length reduces to about 35 nm, the high interface resistivity and low layer thermal conductivity of SL TFs caused by these size effects lead to very low thermal conductivity. For SL TFs with certain periodic lengths, their thermal conductivity is even lower than those of SL NWs of ultrasmall diameters. The relationship between the cumulative thermal conductivity and phonon wavelength is applied in this study to explain the change in interface resistivity, layer thermal conductivity, and periodic length for the minimum thermal conductivity as the specimen and periodic lengths change. The results presented here are important to understand the limits of scaling of superlattice materials for thermal applications.

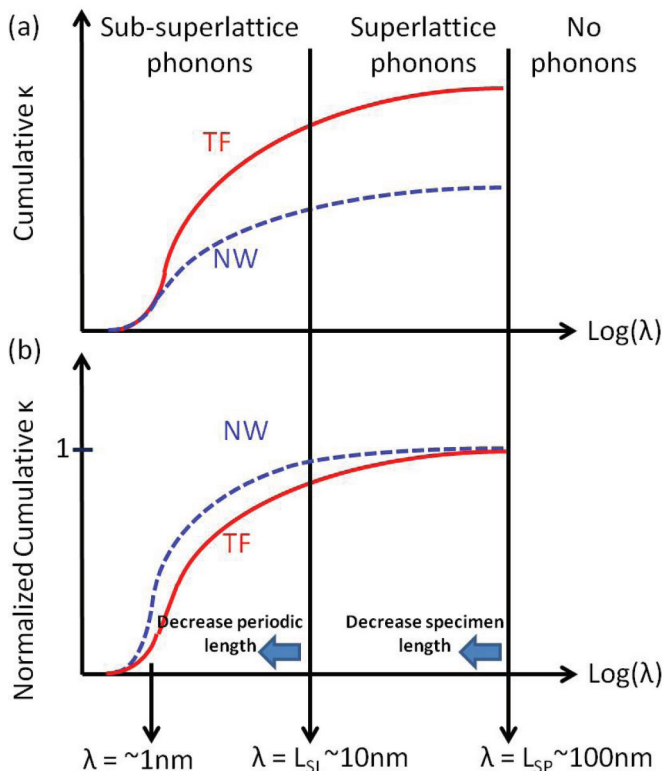


FIG. 9. (Color online) Schematic (a) cumulative thermal conductivity and (b) normalized cumulative thermal conductivity of superlattice thin films (solid lines) and nanowires (dashed lines). L_{SP} is the specimen length, and L_{SL} is the periodic length of superlattice.

ACKNOWLEDGMENTS

The authors would like to thank M. Lundstrom, C. Jeong, and A. Shakouri for useful discussions. This work was supported by the US National Science Foundation through Grants No. EEC-0634750 (Network for Computational Nanotechnology) and No. ECCS-1028667. Computational resources from nanoHUB.org are gratefully acknowledged.

- ¹A. I. Boukai, Y. Bunimovich, J. Tahir-Kheli, J. K. Yu, W. A. Goddard, and J. R. Heath, *Nature (London)* **451**, 168 (2008).
- ²A. I. Hochbaum, R. Chen, R. D. Delgado, W. Liang, E. C. Garnett, M. Najarian, A. Majumdar, and P. Yang, *Nature (London)* **451**, 163 (2008).
- ³A. Shakouri and M. Zebarjadi, in *Thermal Nanosystems and Nanomaterials*, edited by S. Volz (Springer, Berlin, 2009), p. 225.
- ⁴M. S. Dresselhaus, G. Chen, M. Y. Tang, R. G. Yang, H. Lee, D. Z. Wang, Z. F. Ren, J. P. Fleurial, and P. Gogna, *Adv. Mater.* **19**, 1043 (2007).
- ⁵A. J. Minnich, M. S. Dresselhaus, Z. F. Ren, and G. Chen, *Energy Environ. Sci.* **2**, 466 (2009).
- ⁶R. Venkatasubramanian, E. Siivola, T. Colpitts, and B. O'Quinn, *Nature (London)* **413**, 597 (2001).
- ⁷T. Borca-Tasciuc, W. L. Liu, J. L. Liu, T. F. Zeng, D. W. Song, C. D. Moore, G. Chen, K. L. Wang, M. S. Goorsky, T. Radetic, R. Gronsky, T. Koga, and M. S. Dresselhaus, *Superlattices Microstruct.* **28**, 199 (2000).
- ⁸S. Chakraborty, C. A. Kleint, A. Heinrich, C. M. Schneider, J. Schumann, M. Falke, and S. Teichert, *Appl. Phys. Lett.* **83**, 4184 (2003).
- ⁹L. J. Lauhon, M. S. Gudiksen, and C. M. Lieber, *Philos. Trans. R. Soc. London A* **362**, 1247 (2004).
- ¹⁰L. J. Lauhon, M. S. Gudiksen, C. L. Wang, and C. M. Lieber, *Nature (London)* **420**, 57 (2002).
- ¹¹M. Law, J. Goldberger, and P. D. Yang, *Annu. Rev. Mater. Res.* **34**, 83 (2004).
- ¹²S. M. Lee, D. G. Cahill, and R. Venkatasubramanian, *Appl. Phys. Lett.* **70**, 2957 (1997).
- ¹³D. Y. Li, Y. Wu, R. Fan, P. D. Yang, and A. Majumdar, *Appl. Phys. Lett.* **83**, 3186 (2003).
- ¹⁴C.-K. Liu, C.-K. Yu, H.-C. Chien, S.-L. Kuo, C.-Y. Hsu, M.-J. Dai, G.-L. Luo, S.-C. Huang, and M.-J. Huang, *J. Appl. Phys.* **104**, 144301 (2008).
- ¹⁵X. W. Wang, H. Lee, Y. C. Lan, G. H. Zhu, G. Joshi, D. Z. Wang, J. Yang, A. J. Muto, M. Y. Tang, J. Klatsky, S. Song, M. S. Dresselhaus, G. Chen, and Z. F. Ren, *Appl. Phys. Lett.* **93**, 193121 (2008).
- ¹⁶J. Baxter, Z. X. Bian, G. Chen, D. Danielson, M. S. Dresselhaus, A. G. Fedorov, T. S. Fisher, C. W. Jones, E. Maginn, U. Kortshagen, A. Manthiram, A. Nozik, D. R. Rolison, T. Sands, L. Shi, D. Sholl, and Y. Y. Wu, *Energy Environ. Sci.* **2**, 559 (2009).
- ¹⁷Y. P. He and G. Galli, *Phys. Rev. Lett.* **108**, 215901 (2012).
- ¹⁸H. R. Shanks, P. H. Sidles, P. D. Maycock, and G. C. Danielson, *Phys. Rev.* **130**, 1743 (1963).
- ¹⁹J. Chen, G. Zhang, and B. W. Li, *Appl. Phys. Lett.* **95**, 073117 (2009).
- ²⁰Y. F. Chen, D. Y. Li, J. R. Lukes, Z. H. Ni, and M. H. Chen, *Phys. Rev. B* **72**, 174302 (2005).
- ²¹M. V. Simkin and G. D. Mahan, *Phys. Rev. Lett.* **84**, 927 (2000).
- ²²J. Garg, N. Bonini, and N. Marzari, *Nano Lett.* **11**, 5135 (2011).
- ²³V. Rawat, Y. K. Koh, D. G. Cahill, and T. D. Sands, *J. Appl. Phys.* **105**, 024909 (2009).
- ²⁴R. Venkatasubramanian, *Phys. Rev. B* **61**, 3091 (2000).
- ²⁵Y. S. Ju and K. E. Goodson, *Appl. Phys. Lett.* **74**, 3005 (1999).
- ²⁶A. J. Minnich, J. A. Johnson, A. J. Schmidt, K. Esfarjani, M. S. Dresselhaus, K. A. Nelson, and G. Chen, *Phys. Rev. Lett.* **107**, 095901 (2011).
- ²⁷P. K. Schelling, S. R. Phillpot, and P. Keblinski, *Phys. Rev. B* **65**, 144306 (2002).
- ²⁸G. Balasubramanian and I. K. Puri, *Appl. Phys. Lett.* **99**, 013116 (2011).
- ²⁹V. Samvedi and V. Tomar, *Nanotechnology* **20**, 365701 (2009).
- ³⁰Available from <http://lammps.sandia.gov/>
- ³¹K. J. Ding and H. C. Andersen, *Phys. Rev. B* **34**, 6987 (1986).
- ³²F. H. Stillinger and T. A. Weber, *Phys. Rev. B* **31**, 5262 (1985).
- ³³S. C. Jain and W. Hayes, *Semicond. Sci. Technol.* **6**, 547 (1991).
- ³⁴A. Arumbakkam, E. Davidson, and A. Strachan, *Nanotechnology* **18**, 345705 (2007).
- ³⁵F. Müller-Plathe, *J. Chem. Phys.* **106**, 6082 (1997).
- ³⁶I. Ponomareva, D. Srivastava, and M. Menon, *Nano Lett.* **7**, 1155 (2007).
- ³⁷Y. Zhou, B. Anglin, and A. Strachan, *J. Chem. Phys.* **127**, 184702 (2007).
- ³⁸See Supplemental Material at <http://link.aps.org/supplemental/10.1103/PhysRevB.87.115302> for details.
- ³⁹D. Donadio and G. Galli, *Phys. Rev. Lett.* **102**, 195901 (2009).
- ⁴⁰S. G. Volz and G. Chen, *Phys. Rev. B* **61**, 2651 (2000).
- ⁴¹A. S. Henry and G. Chen, *J. Comput. Theor. Nanosci.* **5**, 141 (2008).
- ⁴²C. Jeong, S. Datta, and M. Lundstrom, *J. Appl. Phys.* **109**, 073718 (2011).
- ⁴³C. J. Glassbrenner and G. A. Slack, *Phys. Rev.* **134**, A1058 (1964).
- ⁴⁴P. E. Hopkins, C. M. Reinke, M. F. Su, R. H. Olsson, E. A. Shaner, Z. C. Leseman, J. R. Serrano, L. M. Phinney, and I. El-Kady, *Nano Lett.* **11**, 107 (2011).
- ⁴⁵P. Nath and K. L. Chopra, *Phys. Rev. B* **10**, 3412 (1974).
- ⁴⁶J. Chen, G. Zhang, and B. W. Li, *J. Chem. Phys.* **135**, 204705 (2011).
- ⁴⁷K.-H. Lin, S. Sullivan, M. J. Cherukara, A. Strachan, T. Feng, X. Ruan, and B. Qiu, nanoMATERIALS nanoscale heat transport (2011), at <http://nanohub.org/resources/nmstthermal> (DOI: 10.4231/D34Q7QQ1V).
- ⁴⁸M. N. Luckyanova, J. Garg, K. Esfarjani, A. Jandl, M. T. Bulsara, A. J. Schmidt, A. J. Minnich, S. Chen, Mildred. S. Dresselhaus, Z. Ren, E. A. Fitzgerald, and G. Chen, *Science* **338**, 936 (2012).